Mechanical Properties of Nanoparticle Chain Aggregates by Combined AFM and SEM: Isolated Aggregates and Networks

Weizhi Rong,[†] Weiqiang Ding,[‡] Lutz Mädler,[†] Rodney S. Ruoff,[‡] and Sheldon K. Friedlander*,[†]

Chemical and Biomolecular Engineering Department, University of California at Los Angeles, Los Angeles, California 90095, and Department of Mechanical Engineering, Northwestern University, Evanston, Illinois 60208

ABSTRACT

Mechanical properties of nanoparticle chain aggregates (NCA) including tensile strength and Young's modulus were measured using an instrument incorporating an AFM tip under SEM imaging. The NCA were studied individually and as network films. Carbon NCA were made by laser ablation of graphite, and SnO_2 NCA were made by oxidation of a tin compound. The films were deformable and showed elastic behavior. NCA serve as reinforcing fillers in rubber and films of SnO_2 NCA for trace gas detection.

Nanoparticle chain aggregates (NCA) are generated frequently in high-temperature processes. Examples include industrial and laboratory aerosol reactors and the combustion of carbonaceous fuels. They are branched structures composed of primary particles with diameters ranging from 1 to 50 nm. The mechanical properties of NCA are important in the manufacture of composite materials such as reinforced rubber[1] and the fabrication of sensor films,[2] nanoparticle catalyst films,[3] and planarization agents.[4] NCA also play a major role in air pollution.[5]

The use of NCA as reinforcing fillers in rubber and other polymeric materials results in improved mechanical properties including increased tensile strength, Young's modulus, and tear strength. In the formulation of a rubber tire tread, the fillers may constitute 20−30% by weight. The mechanism by which reinforcing fillers enhance the mechanical properties of elastomers is not well understood, but it may result from filler−filler interaction[6] and the interaction between rubber polymer molecules and filler networks.[1,7−9] Although much is known about the behavior of polymer molecules, much less is known about NCA mechanical properties.[6,10,11]

Elastomers are characterized by their large deformability with essentially complete reversibility. Friedlander et al.[12−16] have demonstrated that the filler aggregates have a remarkable deformability and elasticity. Mark and his co-workers[11,17,18] have also suggested that elastomer components must be joined into a network structure to achieve enhanced elasticity. Compared with an isolated chain, a chain in a network will be entangled and cross-linked with its neighbors. The entanglements and cross links of network chains will restrain the movement and deformation of each chain, leading to a more stable and recoverable structure.[19,20] A well-known reinforcing filler, carbon black, also forms aggregate networks in filled rubber.[6,10,21] The filler network also plays an important role in enhancing the elastic behavior of filled elastomers. A better understanding of the nanoscale mechanical properties of the aggregate filler itself, such as the breaking force, tensile strength, Young's modulus, and the dynamic behavior of the aggregate networks, may help to explain the reinforcing mechanism of the filler−elastomer nanocomposite system.

Flexible NCA films are also of interest because of their potential applications to deformable electronic surfaces.[22] The film needs to adjust to the deformation of the underlying substrate and should return to the original state, without altering its performance. Furthermore, besides stability, certain applications require a high porosity of the coating structure for better surface accessibility, as in sensor[23,24] and catalyst coatings.[25] The two requirements of high stability and porosity are difficult to achieve at the same time by ordinary structures. NCA coatings generally have a high porosity, which has been shown by both experiments[2] and

* To whom correspondence should be addressed. E-mail: skf@ucla.edu.
† University of California at Los Angeles.
‡ Northwestern University.

numerical simulations.[26] Studies of the dynamic behavior of NCA networks may help determine whether coatings composed of aggregates will be useful in fabricating deformable electronic surfaces.

According to modern usage, *agglomerates* are assemblies of *aggregates* held together by weak bonds that may be due to van der Waals forces or by ionic/covalent bonds operating over very small contact areas.[5,27] In contrast, *aggregates* are assemblies of primary particles held together by strong bonds, probably ionic/covalent in nature. In this study, we define "contact force" as the force between attached aggregates forming agglomerates. The "breaking force" is defined as the strong force between primary particles forming aggregates. Often contact and breaking forces are lumped together, making it difficult to predict aggregate and agglomerate formation/breakage and dynamic behavior. Specific information on aggregate and agglomerate strength is important in many nanoparticle applications, such as dispersants of cohesive particles,[28] pharmaceutical powder inhalers,[29] and packing of fine particles.[30]

Experimental studies have shown that NCA made of various materials can be strained up to 100%; after breaking, the broken segments of the aggregate contract rapidly to more compact structures, indicating elastic NCA behavior.[12,13,16,31] The transmission electron microscope (TEM) and the atomic force microscope (AFM) have been used to study NCA behavior and their mechanical properties in several ways:

(a) TEM grid:[13] In the first study of NCA stretching, NCA of various materials were deposited on TEM grids and observed in the electron microscope; aggregates were stretched by the motion of the edges of holes that formed in the carbon/Formvar film on the TEM grid. Aggregates lying across the film holes stretched, broke, and contracted as the holes widened. (b) TEM + NSMD:[12,15] To conduct a better controlled study of NCA stretching and contraction, a novel nanostructure manipulation device (NSMD) was designed and fabricated, which made it possible to apply tension to nanostructures mounted in the TEM. In these NSMD studies, stretching caused initially folded NCA to reorganize into a taut configuration. Further stretching either led to chain breakage with fast recoil of the broken segments or to a partial elastic behavior of the chain at small strains. (c) AFM: Rong et al.[16] made the first studies of the breaking and stretching of carbon NCA using AFM force spectroscopy, stretching aggregates between a cantilever tip and an aggregate-coated substrate. The tensile strength and Young's modulus of carbon NCA were estimated and compared with bulk values.

However, conventional AFM force spectroscopy does not have microscopic capability sufficient to observe details of the structure of the stretched chain. The goal of the current study is to combine the observational capability of electron microscopy with AFM force measurements in the same measurement system to study NCA dynamics quantitatively. For this purpose, an AFM method in conjunction with scanning electron microscopy ("AFM + SEM") was used to simultaneously image structural changes in NCA and make real-time measurements of the stretching/breaking forces.

For AFM + SEM observation, NCA were deposited on two types of substrates: half-cut TEM grids (3 mm in diameter) and silicon substrates of similar size. The substrate was mounted inside the AFM + SEM system; NCA deposited on the substrate were picked up by a movable AFM cantilever tip. The aggregate was stretched until it broke and the broken segment recoiled. The entire stretching and breaking process was observed and recorded in the SEM. From SEM image analysis and the AFM cantilever calibrations, the tensile load and strain were obtained for each recorded loading state. Details of the experimental procedure are described in what follows:

Two types of NCA were studied. Carbon NCA were generated by laser ablation (Figure 1 a).[32,33] Targets composed of graphite (spectroscopic grade, Ted Pella Inc.) in the form of 2-mm-thick disks, 25.4 mm in diameter, were ablated using a YAG laser (Hughes Aircraft Co., MDIVAD Laser Rangefinder) in an Ar atmosphere. The average laser power was about 100 mJ/pulse, with a pulse frequency of 10 Hz. NCA in the carrier gas (Argon, purity = 99.999%, Air Liquide America Corp., 1 L/min) exiting the laser ablation chamber were deposited on a TEM grid (400 mesh copper, carbon film, Electron Microscopy Sciences) placed on a membrane filter (Pore size 8.0 μm, Millipore, Type SC) inside a chamber (TEM grid chamber in Figure 1a). The number concentration of the aggregates in Ar was about 10^7/cm^3, and the sampling time was 20 min. The primary particle size of the aggregates ranged from 25 to 35 nm, and the average length of the aggregates was about 2 μm. An SEM (FEI Nova-600 "Nano SEM") image of several aggregates is shown in Figure 1b. A high-resolution TEM image (Figure 1c) was obtained with a JEOL JEM-100 CX TEM operated at an accelerating voltage of 100 kV. The carbon NCA probably form by the condensation of vaporized graphite, but their atomic structure is not known.

SnO$_2$ particles deposited as porous films on chips are used widely to detect toxic gases like CO and NO$_x$.[2,23,24] SnO$_2$ NCA were generated by flame spray pyrolysis (FSP) using an apparatus that consisted of a nozzle surrounded by a flamelet ring (Figure 1d).[34] The liquid precursor, 0.4 M tin (II) 2-ethylhexanoate (purity stated as 99.95%, Alfa Aesar) in toluene (purity stated as >99.5%, Fisher Scientific) was fed by a syringe pump (KD Scientific Inc.) with a constant feed rate of 4 mL/min. The liquid was dispersed into fine droplets (~10 μm in diameter)[35] with 5 L/min oxygen (Airgas, purity stated as 99.95%) maintaining a pressure drop of 1.5 bar at the nozzle exit. The liquid spray was ignited by the premixed methane/oxygen (1.58 L/min and 1.38 L/min, respectively) flamelet ring surrounding the nozzle exit. An oxygen sheath flow (5 L/min) was supplied through a sintered metal plate ring (width 8 mm, inner radius 9 mm). The NCA were directly deposited by thermophoresis on a silicon substrate (0.5 mm in thickness and 5 mm x 10 mm in shape, Department of Physics, University of Karlsruhe) or a TEM grid (400 mesh copper, carbon film, Electron Microscopy Sciences) mounted on a water-cooled copper block equipped with a K-type thermocouple (Omega) to control substrate temperature during deposition. The substrate
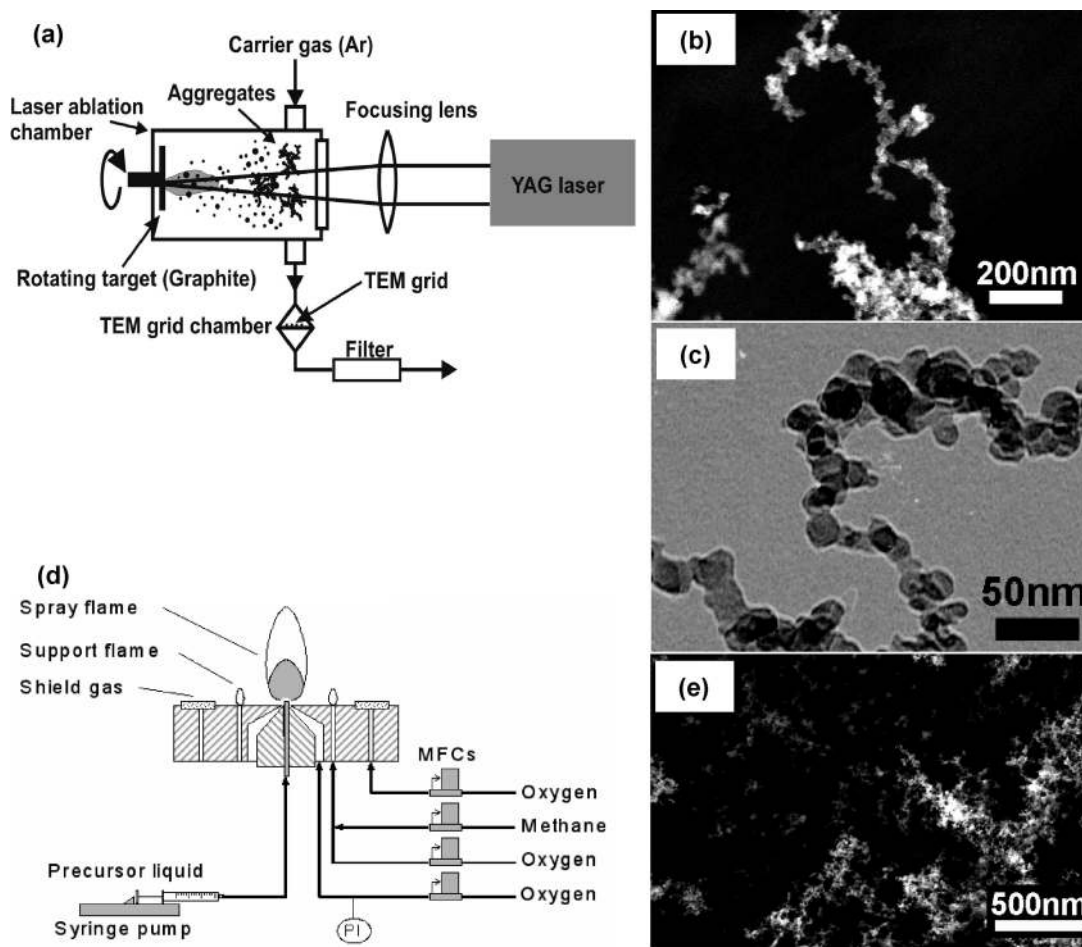
Figure 1. (a) Laser ablation system for generating carbon NCA. The rotating target was ablated by a laser beam, forming a vapor plume (gray area in the figure)[32,33] (b) A SEM image of typical carbon aggregates generated by laser ablation. (c) A TEM image of carbon aggregates generated by laser ablation. (d) Flame spray pyrolysis for generating SnO_2 NCA.[34] (e) A SEM image of typical SnO_2 aggregates generated by flame spray pyrolysis.

temperature was maintained at 120 °C to avoid water condensation on the substrate and sample. The deposition substrate was centered 200 mm above the nozzle. The sampling time was 10 s. The primary particle size of the SnO_2 NCA ranged from 15 to 25 nm, and the length of the aggregates ranged from 0.5 to 2 μm. An SEM image of several aggregates is shown in Figure 1e.

Nanoscale tensile tests on the NCA were performed with a specially designed nanomanipulator[36–41] inside the vacuum chamber of a FEI Nova-600 SEM (a variable pressure field emission gun SEM). Two AFM cantilever tips were mounted on the two opposing positioning stages of the manipulator (Figure 2a): The soft force-sensing cantilever (CSC 12, length 350 μm, nominal force constant 0.03 N/m, Mikro-Masch Inc.) was mounted at the end of a piezoelectric bender (Noliac A/S, Denmark, ceramic multilayer bender B1) on the X−Y linear motion stage; the rigid cantilever (NSC 12, length 90 μm, nominal force constant 14.0 N/m, MikroMasch Inc.) was mounted on the Z linear motion stage, together with the NCA source substrate (Figure 2b).

The spring constant of the force-sensing (relatively soft) AFM cantilever was calibrated inside the SEM vacuum chamber prior to the test, with a resonance method developed by Sader et al.[42] A detailed description of the calibration procedure has been reported elsewhere.[36]

Through nanomanipulation, the sharp tip of the soft AFM cantilever was brought into contact with one end of a selected NCA protruding from the source substrate (Figure 3 a). A clamp was fabricated using an electron-beam-induced deposition (EBID) method to attach the chain to the AFM tip. EBID is a method, by irradiation with an electron beam, of decomposing molecules to make a deposit on a substrate; Ruoff et al.[36–41] have pioneered its use to construct nanoscale clamps on a specific site inside a SEM. While focusing the electron beam on a certain area on the substrate surface, the secondary electrons generated through primary electron-substrate interaction probably decomposed residual hydro-carbon molecules adsorbed on the substrate and formed a local deposit.[36,37] In this study, EBID was used to clamp each NCA tested to the AFM tip. The clamped chains never detached from the tip in the experiments performed.

Because of the relatively large depth of focus of SEM, it is non-trivial to eliminate height mismatch in our nanoscale tensile study inside the SEM. We used the following steps to reduce height mismatch: First, we zoomed in to the EBID clamp on the AFM tip that is attached to the X−Y stage,
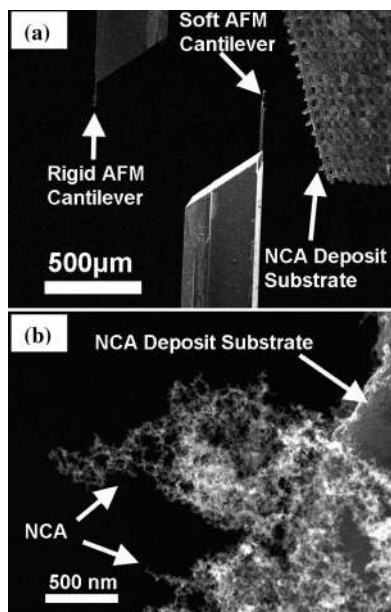
Figure 2. (a) SEM image of the experimental setup for tensile strength measurement: the NCA deposit substrate (a half-cut TEM grid) and AFM cantilevers mounted on the home-built nanomanipulator. (b) SEM image of the NCA deposit on the edge of the substrate. The protruding chains are used for the tensile experiment.

and adjusted the focus (working distance of the electron beam) to bring the clamp into focus. Then, we zoomed in to the other EBID clamp (on the AFM tip that was attached to the Z stage) and adjusted the height of the Z stage to bring the clamp into focus. This way, both ends of the NCAs are "more or less" at the same height level. Because the depth of focus of SEM is inversely proportional to the magnification, we always "zoomed in" at high magnification (>100 000×) during such adjustments to minimize the height mismatch. The effect of potential height mismatch on our measurement results is discussed in more detail later. The clamped NCA was subjected to tension by applying a series of voltages to the piezoelectric bender (Noliac A/S, Denmark, ceramic multilayer bender B1) that manipulated the motion of the soft AFM cantilever. The NCA was stretched between the tip and the source until the chain broke. The breaking force and tensile strength were calculated for each NCA tested.

To obtain well-defined stress/strain relations for isolated aggregates, the two opposing AFM tips were used to stretch the two ends of carbon NCA. First, the soft AFM tip was used to pick a protruding aggregate from the deposit and stretch it until it broke. After breakage, one of the broken segments was still attached to the AFM tip. The loose end of this segment was clamped to the rigid AFM cantilever tip using EBID clamping. Then, the soft cantilever was gradually moved away from the rigid cantilever by actuating the piezoelectric bender. As a result, tension was applied to the NCA segment. The rigid cantilever, with a much larger spring constant than the soft cantilever, is assumed to be approximately static during stretching.

In our current experimental setup, we did not measure tensile load or the strain directly during the loading process. With the *movie recording function* of the FEI SEM, a series
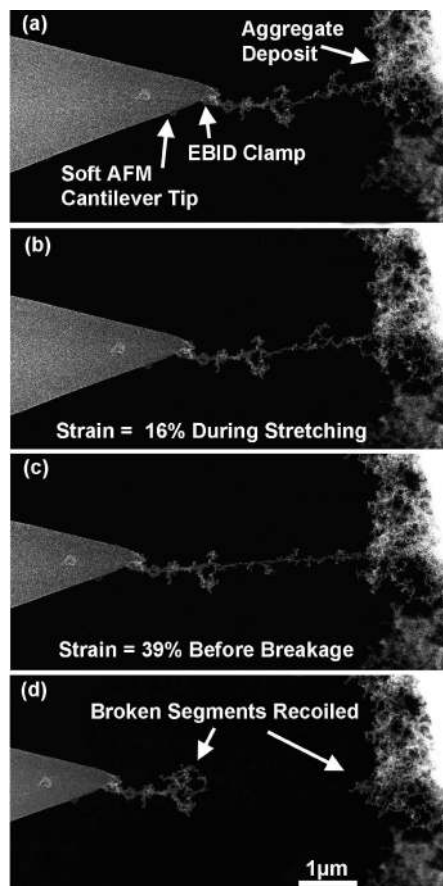

Figure 3. SEM images of the stretching of carbon NCA using the AFM tip. The scale bar applies to all images. (a) The protruding aggregate was clamped on the AFM cantilever tip. (b) The tip was moved away from the aggregate source, straining the aggregate 16%. (c) Strain of 39%. (d) The aggregate broke and the broken segments recoiled.

of SEM images was automatically acquired and saved during the tensile loading process. The tensile load and strain were obtained from image analysis after the experiment was finished. Knowing the cross-sectional area, the tensile stress was calculated. The stress−strain curve was then plotted, from which the Young's modulus of the carbon NCA was estimated. The detailed data analysis is described elsewhere.[43]

Figure 3 shows a NCA clamped to the AFM tip that was pulled from the substrate until it broke at a maximum strain of about 39%. During the test, a dc voltage increased in discrete steps was applied to the piezoelectric bimorph to move the soft AFM tip away from the deposit substrate. The average rate of the AFM tip movement during stretching ranged from 50 to 80 nm/s. The actual stretching rate was much higher because the tensile load was increased in discrete steps, and the response of the piezoelectric bender to the applied dc voltage was fast (the manufacturer states that the response is in the millisecond range). The actual strain rate is unknown because we do not know the exact response time of the piezoelectric bender, but it should be on the order of 0.1 s^{-1}. After breakage, the broken segments recoiled quickly toward their respective ends.

Tensile strength (*TS*) is a measure of the ability of a material to resist stretching forces. It is obtained by dividing
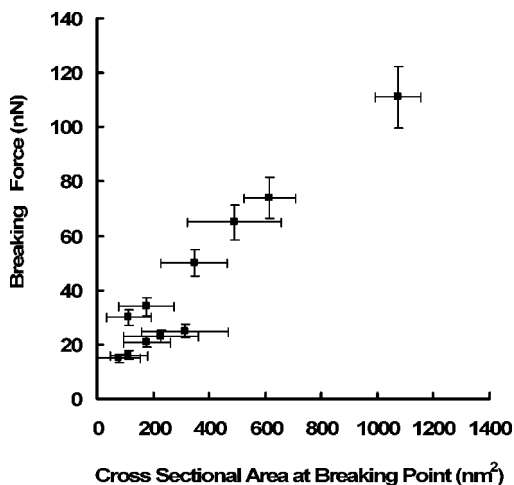
Figure 4. Relationship between the breaking force and the cross-sectional area at the breaking point of 11 different isolated carbon NCA. The breaking force was approximately proportional to the cross-sectional area where the chain broke. The average tensile strength was 0.15 ± 0.03 GPa.

the maximum load a body can bear before breaking (F_{break}) by the cross-sectional area (A) at the break point

$$TS = \frac{F_{break}}{A} \qquad (1)$$

The force at breaking, $F_{break,}$ can be calculated by analyzing the displacement of the AFM cantilever, and A is estimated from the SEM image.

In a previous study, NCA were assumed to behave like wires with uniform cross sections and the diameters of the wires were set equal to the average diameter of the primary particles of the NCA.[16] However, NCA are composed of primary particles with different sizes and the adjoining primary particles form narrow necks between each other. The diameter of the cross section of the neck was always smaller than the primary particle diameters. Consequently, the necks between primary particles are the narrowest and probably the weakest part of the chain aggregate. This is in agreement with a high-resolution TEM study, which showed that the stretched NCA broke at the neck between two adjoining primary particles.[15] Our real-time SEM imaging allowed us to measure the diameter of the neck (d) where the NCA broke. The cross section (A), assumed circular, is $\pi \cdot d^2/4$.

In this study, the breaking forces and cross-sectional areas of each neck at the point of NCA breaking were determined for 11 different NCA. The results are plotted in Figure 4. In this way, we have for the first time obtained a relationship between the stretching force needed to break the NCA and the cross-sectional area at the breaking point. The larger neck size resulted in a larger NCA breaking force. The breaking force, F_{break}, and cross-sectional area, A, were approximately linearly related, indicating that the tensile strength of the carbon NCA is roughly constant. The tensile strength of each individual carbon NCA was obtained using eq 1. The average tensile strength was 0.15 ± 0.03 GPa. Because of the limitation of the SEM resolution, the error in the cross-sectional

area was considerable, especially when the diameter of the neck cross section was less than 20 nm. The error bar was determined by the pixel resolution of the recorded SEM image.

The structure of the carbon in the NCA formed in this study is not known. The measured tensile strength of the NCA is much larger than literature bulk values for graphite (0.003−0.03 GPa),[44,45] but we were unable to find data for amorphous carbon. These experiments indicate that the forces that hold the chain aggregate together are approximately proportional to the cross-sectional area of the necks.

The tensile strength of carbon NCA estimated in our earlier AFM study (0.0045 ± 0.0025 GPa)[16] was much smaller than the current results: (1) The previous AFM study did not provide simultaneous imaging of the NCA stretching/breaking. Therefore, forces recorded in this study may result from the rearrangements of the primary particles (such as unfolding kinks) or the detachment of aggregates from the AFM tip or from other aggregates in an agglomerate rather than the actual breakage. (2) Furthermore, the NCA primary particle sizes in the previous study were generally smaller than those of this study. In our earlier study, it was assumed that NCA behave like fibers of uniform cross sections. This results in an overestimation of the cross-sectional area (eq 1), and underestimation of the tensile strength. (3) Finally, in the previous AFM study, NCA were stretched in ambient air at room temperature but this study was made inside the SEM vacuum chamber where the high-intensity electron beam was focusing on the NCA during the operation. The specific effects of the vacuum environment and the electron beam on the measured NCA mechanical properties are not well understood and also have not been discussed in detail in other published studies.[39]

Young's modulus (E) is a measure of the resistance of a material to deformation. In the same manner, we define the NCA Young's modulus, which is determined from the slope of the linear part of the stress−strain curve created by SEM image analysis, in a region of elastic behavior (reversibility).

Figure 5 shows the stretching and breaking of a carbon NCA mounted between two opposing AFM tips. Two particles on the chain were chosen as reference points (p and q). The distance between them was measured for each loading state, and the strain was calculated. The segment pq, located in the middle of the aggregate, was studied. We did not choose the entire aggregate because the end segments of the aggregate, close to the location that was clamped onto the AFM tip, might be affected by the EBID deposition occurring during the clamping of the aggregates to the AFM tips. The tensile stress calculated was the ratio of stretching force to cross-sectional area. The force was calculated using the method described previously. In the calculation of Young's modulus, we assumed that the chain behaves like a wire with a uniform cross section. The diameter of the cross-sectional area was set equal to the average diameter of the primary particles and the necks. This may cause an error because the primary particle diameters differ. However, the Young's modulus referred to here is an average measure of the entire aggregate and corresponds to an effective value.
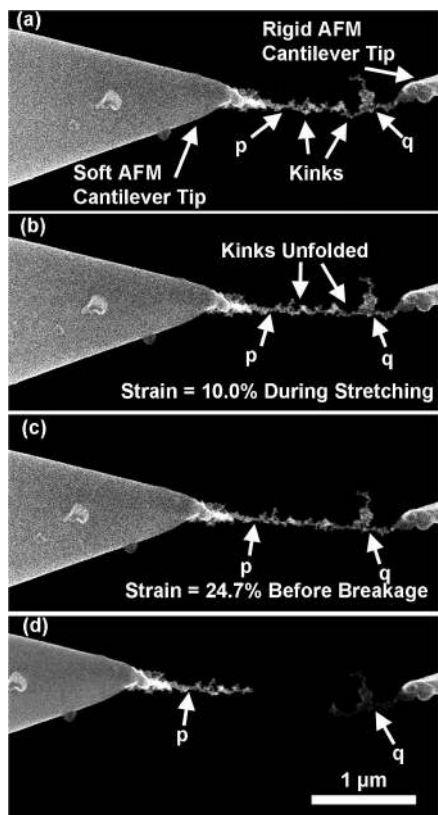
Figure 5. Stretching of an isolated carbon NCA using two opposing AFM cantilever tips. From a to b, the aggregate was stretched and the kinks along the aggregate were straightened. From b to c, the taut chain was stretched further. Points p and q denote a segment of the aggregate.

Three isolated NCA were studied using the two opposing AFM tips. Figure 6a shows the stress and strain measured during the stretching pictured in Figure 5. Similar stress−strain curves were obtained for the three NCA. The curves showed a similar trend compared with a hypothetical stress−strain curve (Figure 6b) constructed based on previous observations of NCA stretching.[12] The stress−strain curves can be divided into three stages (Figure 6a and b):

In stage I, chain kinks on the scale of a few particle diameters straightened by rotation and/or sliding at particle−particle interfaces (Figure 5a to b, Figure 6 point A to B). Rotation and/or sliding are relatively low-energy processes that lead to large changes in the linear dimension of the NCA as kinks straighten. We refer to this step as reorganization of the folded chain into a straight, taut configuration. We believe that this stage is irreversible.

Stage II (Figure 5b to c, Figure 6 point B to C) is an elastic domain, where a comparatively larger stress is required to strain the taut aggregate. As strain increases, the stress rises much faster in stage II than in stage I. A previous TEM study[12] showed that in stage II the subsequent reduction in tension caused the chain under small strain to contract (almost to the original length), retaining a nearly straight configuration as expected for elastic behavior. This implies a partial reversibility of the strain under stretching and contraction. The slope of the stress−strain curve in stage II is the Young's modulus of the carbon NCA. The observed strain range of stage II (Figure 6a) was much wider than

that in the hypothetical curve (Figure 6b) because the NCA studied were not ideal uniform single chains, but complex aggregates with branches. Even along the same chain, different structures (primary particles and necks) and primary particle sizes are present. It is possible that within the same NCA most segments undergo elastic behavior in stage II, but others are still in stage I (straightening some strong kinks that were not fully unfolded) or III (some narrow necks were already stretched over the elastic limit). The overall NCA behavior results from the combination of elastic and plastic properties in different regions along the chain.

Stage III (Figure 5c to d, Figure 6 point D) is a plastic domain, in which some segments of NCA were stretched above the elastic limit. Further stretching broke the NCA at its weakest point, at which the tensile strength was exceeded. The breakage led to the elastic recovery of the aggregate. This behavior is comparable with the fracture of macroscale elastic materials.[46] Strain energy stored in the aggregate segments in the elastic region led to the fast contraction of the two broken sections of the chain, which we have observed many times using different methods.[12,14−16]

The stress−strain curves were used to estimate the tensile properties of the carbon NCA such as tensile strength (maximum stress), failure strain (maximum strain), and the Young's modulus (slope in stage II) (see Table 1).

Data based on the recorded SEM images were analyzed without considering possible height mismatch between the two EBID clamps. As discussed previously, due to the relatively large depth of focus in scanning electron microscopy, there may be a height mismatch between the two clamps after the height-adjustment process. The height mismatch leads to a lower measured tensile load and a higher measured strain, which results in lower values for the tensile strength and Young's modulus. Under the worst situation, the height mismatch between the two EBID clamps equals the depth of focus at that specific imaging condition. The maximum possible depth of focus during our adjustment is around 667 nm (100 000x magnification, 30 μm aperture diameter, 5.0 mm working distance).[47] A second analysis was performed considering this maximum ("worst case scenario") height mismatch, and the corresponding results are listed in Table 1 and shown in Figure 6c. Because we do not know the exact height mismatch, the results assuming zero and maximum height mismatch set the lower and upper bounds of the true values.

The strains at which failure occurred for carbon NCA (8.4−24.7%) were generally smaller than values reported earlier (20−60%)[12] because the NCA mounted between the two AFM tips was a broken segment of the longer NCA that had been stretched previously. The NCA studied had fewer kinks and were in a more taut state than those in our previous experiments. Consequently, less strain was needed to stretch and break them. The tensile strengths of the three NCA (0.039−0.099 GPa) were only slightly lower than the results obtained in the previous section from 11 measurements (0.15 ± 0.03 GPa). The cross section at the breaking point for the 11 measurements was determined by SEM analysis, whereas for the three NCA we assumed a
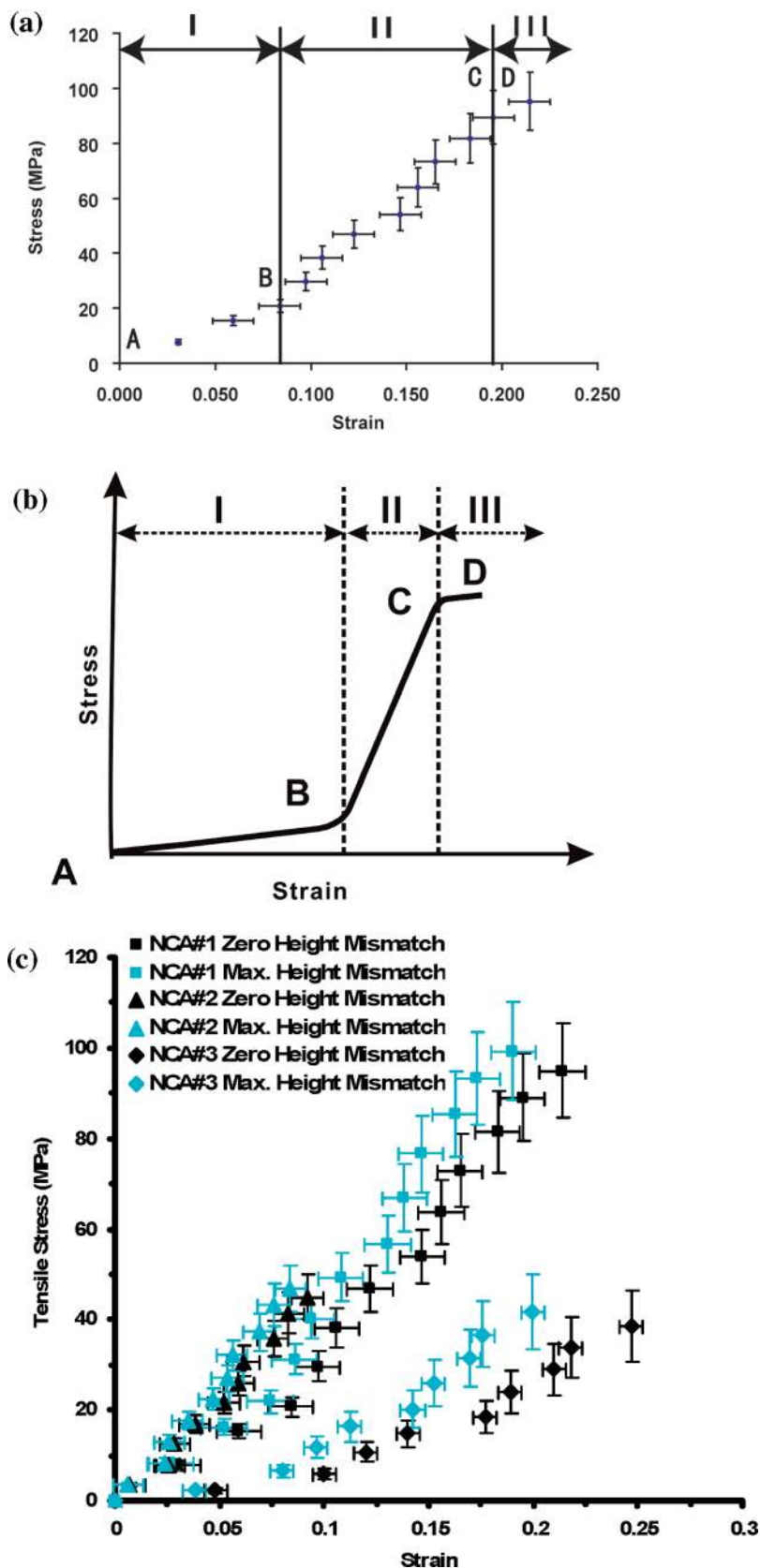
Figure 6. Stress vs strain diagram for carbon chain aggregate stretching. On the basis of observations, it was assumed that stage I corresponds to chain straightening by rotation and grain boundary sliding near primary particle interfaces. Stage II and stage III represent elastic and plastic strain of the primary particles, respectively. (a) Stress and strain measured during stretching shown in Figure 5. (b) Idealized NCA stress−strain curve.[12] (c) Stress−strain curves of three NCAs assuming zero and maximum height mismatch on the same diagram.

Table 1. Tensile Loading Results for Three Carbon NCA

NCA no.	length[c] (μm)	average diameter (nm)	failure strain (zero height mismatch)[a] (%)	failure strain (max height mismatch)[b] (%)	tensile strength (zero height mismatch)[a] (GPa)	tensile strength (max height mismatch)[b] (GPa)	Young's modulus (zero height mismatch)[a] (GPa)	Young's modulus (max height mismatch)[b] (GPa)
1	0.60	26	21.4	19.0	0.095	0.099	0.60	0.70
2	0.88	38	9.2	8.4	0.045	0.047	0.55	0.62
3	1.0	32	24.7	20.0	0.039	0.042	0.22	0.29

[a] Assumed. [b] Assumed. [c] Gauge length between two selected particles, not the entire NCA length.

uniform cross section. This approximation leads to a larger cross-sectional area than the cross-sectional area at the breaking point, resulting in smaller tensile strength values.

Values of the Young's modulus of the three NCA were of the same order of magnitude but larger than our previous AFM results (0.0030 to 0.0088 GPa).[16] The reasons for the difference between the AFM and AFM + SEM studies were discussed in the previous section. The calculated Young's modulus of carbon NCA (0.22 to 0.70 GPa) was over 1 order of magnitude smaller than literature bulk values for isotropic graphite (2.1 to 18.6 GPa)[48] or amorphous carbon (2.8 to 13.1 GPa).[48] Simulation studies have shown that the Young's modulus of NCA along certain crystallographic directions may be smaller than that of the bulk. For example, in a simulation study, the Young's modulus along the [100] direction for a seven-nanoparticle kinked copper aggregate was about one-fifth of the bulk value.[49] This may be caused by a combined effect of the small primary particle diameter (surface effect as discussed in the previous section) and the aggregate kinked structure (discussed previously in the "stage II" section).

In laser ablation, aggregate formation results from an interplay of particle or aggregate collisions and neck formation through sintering. These mechanisms depend on temperature and concentration profiles within the reactors. As a result, aggregate properties are distributed with respect to properties in terms of their primary particle size and neck size. Furthermore, the bonds that hold aggregates may not be uniform at the necks formed by sintering after collision of primary particles. The Young's modulus of aggregates is an average quantity of the entire nonuniform aggregate. This is different from the standard mechanical tests that are conducted on uniform macroscale specimens. Therefore, the Young's modulus of aggregates is an effective property.

We also measured the contact force between carbon particles belonging to two different aggregates. A short aggregate segment was attached to the AFM tip, and the aggregate was brought into contact with another aggregate protruding from the NCA deposit. The AFM tip was then gradually pulled away from the deposit. The two aggregates separated at the original contact point. Three such tests were performed, and the measured carbon aggregate contact forces were of the same order of magnitude, 4, 9, and 12 nN.

Van der Waals forces between two spherical particles can be calculated from the expression[50,51]

$$F_{\mathrm{vdW}} = -\frac{H_a}{6} \frac{64R^6 (h + 2R)}{h^2 (h + 4R)^2 (h^2 + 4Rh + 4R^2)^2} \quad (2)$$

where H_a is the Hamaker constant ($\sim$2.53 $\times$ 10^{-19} J for graphite[52] and $\sim$7 $\times$ 10^{-20} J for amorphous carbon[53]), R is the radius of the primary particles ($\sim$15 nm), and h is the closest gap between the particle surfaces; for particles in contact, the gap (h) is often assumed to be a few angstroms.[5,54] In this study, we used values of h between 2 and 6 Å. This resulted in van der Waals forces ranging from 1 to 8 nN for graphite and 0.2 to 2 nN for amorphous carbon, comparable with the experimental result ($\sim$8 nN).

The contact-force measurement can be considered a first step in the analysis of what holds an agglomerate network structure together. In our measurements, we were able to simulate agglomerate formation by bringing two aggregates into contact. A related problem arises during the fabrication of nanocomposites when agglomerates are broken into aggregates during blending with polymers.[55,56] The agreement found here between measured contact force and calculated van der Waal forces indicates that agglomerates are held together mainly by van der Waals forces. The average contact force between aggregates that we measured ($\sim$8 nN) was much smaller than the average breaking force between the adjoining primary particles of an aggregate ($\sim$46 nN). This supports the idea that the bonds between aggregates in an agglomerate are weaker than the primary particle bonds inside an aggregate.

When we pulled protruding aggregates from the NCA deposit on the substrate (copper TEM grid or silicon), the aggregates stretched and broke instead of being pulled from the deposit. This indicated that aggregates were held tightly in the NCA network. In the previous section, we noted that aggregate−aggregate contact was much weaker than the primary particle bonds inside an aggregate. This indicates that the aggregate must either have many contacts with other aggregates in the deposit or be entangled deeply in the network, resulting in a combined force larger than the aggregate breaking force.

When we pulled and stretched the protruding aggregate (Figure 7 a to c), the network behind the aggregate was also pulled toward the AFM tip. Large-scale rearrangements of aggregate structures inside the network were observed (labeled by the arrows). After the NCA broke, the stretched aggregate structures contracted quickly and returned to their original site. Rearrangements of the aggregates caused by
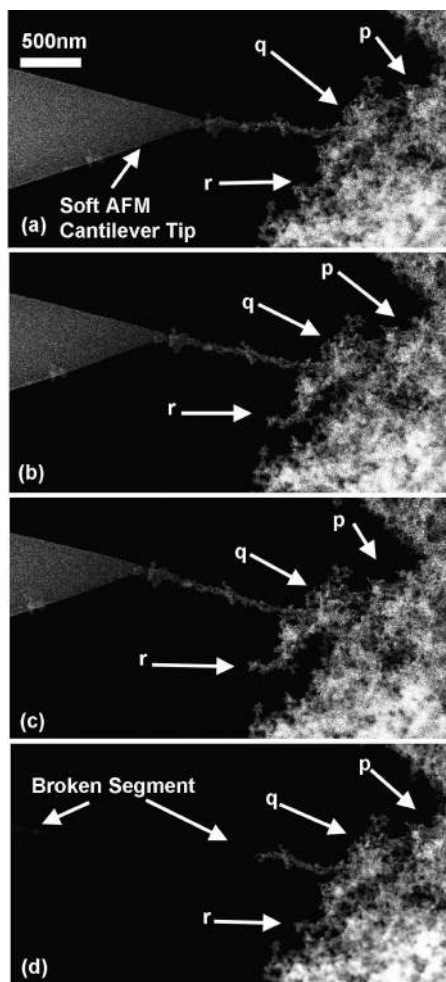
Figure 7. Reversible behavior of carbon NCA network. A portion of the deposit that stretched from a to c after the chain breakage returned to its original position in d. Points p, q, and r denote the network section that returned.

the external stretching force were reversible, which can be seen by comparing parts a and d of Figure 7. Such maneuvers were performed many times with both carbon and SnO_2 NCA, and the same reversible NCA network behavior was observed. This reversibility may shed light on the influence of NCA as reinforcing fillers in elastomers and the potential application of NCA films to the fabrication of deformable electronic surfaces.

Elastomers are characterized by large deformability with near-complete reversibility. The carbon NCA network in our study also showed large deformability and near-complete reversibility, similar to filled elastomers. When these aggregate/agglomerate/networks are within molecular polymer matrices, their deformations and reversibility probably affect the behavior of the filled elastomer. They may contribute to the storage of elastic deformation energy or help cross link and entangle with polymer chains, leading to improved stability and reversibility of the filled elastomer.

The reversible aspects of NCA behavior suggest application to the fabrication of flexible coatings of materials in NCA form. For surfaces subject to flexing, NCA coatings may be able to adjust to the motion of the underlying substrate and return to the original state. Coatings of metal or

metal oxide nanoparticle chain aggregates might assume greater deformation before breaking than homogeneous metal films and recover the film structure when the deformation is removed.

Finally, the combined AFM/SEM system makes possible quantitative study of the mechanical behavior of nanoparticle chain aggregates and networks under tensile stress. The AFM nanomanipulator allows force measurements in the range of nanonewtons while simultaneously the SEM permits visual observation of the strain and the diameter of the neck at which breaking occurred. This permitted the calculation of the tensile strength, the Young's modulus, and the contact force of the NCA. The tensile strength based on measurements with 11 aggregates was 0.15 ± 0.03 GPa. The Young's modulus was $0.22-0.70$ GPa. This is an effective value for the chain averaged over the primary particles and the necks that compose the chain. The reversibility of NCA *networks*, which has not been described before, may provide insight into the mechanism of filler reinforcement in rubber and other elastomers and the potential application of NCA networks to the fabrication of deformable electronic surfaces. Future measurements of interactions between NCA and polymers may be possible with the combined AFM/SEM system.

References

(1) Medalia, A. I.; Kraus, G. In *Science and Technology of Rubber*, 2nd ed.; Mark, J. E., Erman, B., Eirich, F. R., Eds.; Academic: New York, 1994.
(2) Sahm, T.; Mädler, L.; Gurlo, A.; Barsan, N.; Pratsinis, S. E.; Weimar, U. *Sens. Actuators, B* **2004**, *98*, 148−153.
(3) Stark, W. J.; Pratsinis, S. E. *Powder Technol.* **2002**, *126*, 103−108.
(4) Basim, G. B.; Brown, S. C.; Vakarelski, I. U.; Moudgil, B. M. *J. Dispersion Sci. Technol.* **2003**, *24*, 499−515.
(5) Friedlander, S. K. *Smoke, Dust and Haze: Fundamentals of Aerosol Dynamics*, 2nd ed.; Oxford University Press: New York, 2000.
(6) O'Farrell, C. P.; Gerspacher, M.; Nikiel, L. *Kautsch. Gummi Kunstst.* **2000**, *53*, 701.
(7) Gerspacher, M.; O'Farrell, C. P.; Yang, H. H. *Kautsch. Gummi Kunstst.* **1994**, *47*, 349−353.
(8) Payne, A. R. In *Reinforcement of Elastomers*; Kraus, G., Ed.; Wiley: New York, 1965.
(9) Wang, M. J. *Rubber Chem. Technol.* **1999**, *72*, 430−448.
(10) Aminabhavi, T. M.; Cassidy, P. E.; Thompson, C. M. *Rubber Chem. Technol.* **1990**, *63*, 451.
(11) Mark, J. E. *J. Phys. Chem. B* **2003**, *107*, 903−913.
(12) Bandyopadhyaya, R.; Rong, W. Z.; Friedlander, S. K. *Chem. Mater.* **2004**, *16*, 3147−3154.
(13) Friedlander, S. K.; Jang, H. D.; Ryu, K. H. *Appl. Phys. Lett.* **1998**, *72*, 173−175.
(14) Friedlander, S. K.; Ogawa, K.; Ullmann, M. *J. Polym. Sci., Polym. Phys.* **2000**, *38*, 2658−2665.
(15) Suh, Y. J.; Friedlander, S. K. *J. Appl. Phys.* **2003**, *93*, 3515−3523.
(16) Rong, W. Z.; Pelling, A. E.; Ryan, A.; Gimzewski, J. K.; Friedlander, S. K. *Nano Lett.* **2004**, *4*, 2287−2292.
(17) Mark, J. E.; Abou-Hussein, R.; Sen, T. Z.; Kloczkowski, A. *Polymer* **2005**, *46*, 8894−8904.
(18) Pu, Z. C.; Mark, J. E.; Jethmalani, J. M.; Ford, W. T. *Chem. Mater.* **1997**, *9*, 2442−2447.
(19) Mark, J. E. *Macromol. Symp.* **2003**, *201*, 77−83.
(20) Rubinstein, M.; Panyukov, S. *Macromolecules* **2002**, *35*, 6670−6686.
(21) Medalia, A. I. *Rubber Chem. Technol.* **1986**, *59*, 432.

(22) Hsu, P. I.; Huang, M.; Xi, Z.; Wagner, S.; Suo, Z.; Sturm, J. C. *J. Appl. Phys.* **2004**, *95*, 705−712.

(23) Barsan, N.; Stetter, J. R.; Findlay, M.; Gopel, W. *Sens. Actuators, B* **2000**, *66*, 31−33.

(24) Barsan, N.; Weimar, U. *J. Electroceram.* **2001**, *7*, 143−167.

(25) Bell, A. T. *Science* **2003**, *299*, 1688−1691.

(26) Mädler, L.; Lall, A. A.; Friedlander, S. K. *Nanotechnology* **2006**, *17*, 4783−4795.

(27) Bandyopadhyaya, R.; Lall, A. A.; Friedlander, S. K. *Powder Technol.* **2004**, *139*, 193−199.

(28) Yang, J.; Sliva, A.; Banerjee, A.; Dave, R. N.; Pfeffer, R. *Powder Technol.* **2005**, *158*, 21−33.

(29) Coates, M. S.; Chan, H. K.; Fletcher, D. F.; Raper, J. A. *Pharm. Res.* **2005**, *22*, 1445−1453.

(30) Yang, R. Y.; Zou, R. P.; Yu, A. B. *J. Appl. Phys.* **2003**, *94*, 3025−3034.

(31) Suh, Y. J.; Prikhodko, S. V.; Friedlander, S. K. *Microsc. Microanal.* **2002**, *8*, 497−501.

(32) Ogawa, K.; Vogt, T.; Ullmann, M.; Johnson, S.; Friedlander, S. K. *J. Appl. Phys.* **2000**, *87*, 63−73.

(33) Ullmann, M.; Friedlander, S. K.; Schmidt-ott, A. *J. Nanoparticle Res.* **2002**, *4*, 499−509.

(34) Mädler, L.; Kammler, H. K.; Mueller, R.; Pratsinis, S. E. *J. Aerosol Sci.* **2002**, *33*, 369−389.

(35) Mädler, L.; Pratsinis, S. E. *J. Am. Ceram. Soc.* **2002**, *85*, 1713−1718.

(36) Chen, X. Q.; Zhang, S. L.; Dikin, D. A.; Ding, W. Q.; Ruoff, R. S.; Pan, L. J.; Nakayama, Y. *Nano Lett.* **2003**, *3*, 1299−1304.

(37) Ding, W.; Eitan, A.; Fisher, F. T.; Chen, X.; Dikin, D. A.; Andrews, R.; Brinson, L. C.; Schadler, L. S.; Ruoff, R. S. *Nano Lett.* **2003**, *3*, 1593−1597.

(38) Yu, M. F.; Files, B. S.; Arepalli, S.; Ruoff, R. S. *Phys. Rev. Lett.* **2000**, *84*, 5552−5555.

(39) Yu, M. F.; Lourie, O.; Dyer, M. J.; Moloni, K.; Kelly, T. F.; Ruoff, R. S. *Science* **2000**, *287*, 637−640.

(40) Yu, M. F.; Yakobson, B. I.; Ruoff, R. S. *J. Phys. Chem. B* **2000**, *104*, 8764−8767.

(41) Dikin, D. A.; Chen, X.; Ding, W.; Wagner, G.; Ruoff, R. S. *J. Appl. Phys.* **2003**, *93*, 226−230.

(42) Sader, J. E.; Larson, I.; Mulvaney, P.; White, L. R. *Rev. Sci. Instrum.* **1995**, *66*, 3789−3798.

(43) Ding, W.; Calabri, L.; Chen, X.; Kohlhaas, K. M.; Ruoff, R. S. *Compos. Sci. Technol.* **2006**, *66*, 1109−1121.

(44) Perry, R. H.; Green, D. W. *Perry's Chemical Engineers' Handbook*, 7th ed.; McGraw-Hill: New York, 1997.

(45) Reynolds, W. N. *Physical Properties of Graphite*; Elsevier Pub. Co.: Amsterdam, 1968.

(46) Shackelford, J. F. *Introduction to Materials Science for Engineers*, 5th ed.; Prentice Hall: Upper Saddle River, NJ, 2000.

(47) Goldstein, J. *Scanning Electron Microscopy and X-ray Microanalysis*, 3rd ed.; Kluwer Academic/Plenum Publishers: New York, 2003.

(48) Lynch, C. T. *Practical Handbook of Materials Science*; CRC Press: Boca Raton, FL,1989.

(49) Dalis, A.; Friedlander, S. K. *Nanotechnology* **2005**, *16*, S626−S631.

(50) Israelachvili, J. N. *Intermolecular and Surface Forces*, 2nd ed.; Academic Press: London; San Diego, CA, 1991.

(51) Hamaker, H. C. *Physica* **1937**, *4*, 1058−1072.

(52) Dagastine, R. R.; Prieve, D. C.; White, L. R. *J. Colloid Interface Sci.* **2002**, *249*, 78−83.

(53) Dagastine, R. R.; White, L. R.; Jones, P. M.; Hsia, Y. T. *J. Appl. Phys.* **2005**, *97*.

(54) Castellanos, A. *Adv. Phys.* **2005**, *54*, 263−376.

(55) Gerspacher, M.; O'Farrell, C. P.; Yang, H. H. *Kautsch. Gummi Kunstst.* **1994**, *47*, 349−353.

(56) Gerspacher, M.; O'Farrell, C. P. *Kautsch. Gummi Kunstst.* **2001**, *54*, 153−158.